Tropical Waves Are Key Drivers of Extreme Precipitation Events in the Central Sahel

Philippe Peyrillé, Romain Roehrig, Sidiki Sanogo

To cite this version:

Philippe Peyrillé, Romain Roehrig, Sidiki Sanogo. Tropical Waves Are Key Drivers of Extreme Precipitation Events in the Central Sahel. Geophysical Research Letters, 2023, 50 (20), pp.e2023GL103715. 10.1029/2023GL103715 . hal-04259570

HAL Id: hal-04259570
https://hal.science/hal-04259570v1

Submitted on 26 Oct 2023

Tropical Waves are key drivers of Extreme Precipitation Events in the Central Sahel

Philippe Peyrillé[1], Romain Roehrig[1], and Sidiki Sanogo[1,2]

[1]Centre National de Recherches Météorologiques, Météo-France, CNRS, Université de Toulouse, 42 Avenue Coriolis, 31057 Toulouse, France

[2]Institut Pierre-Simon Laplace, Sorbonne université / CNRS, 4 place Jussieu, 75005 Paris, France

Corresponding author: Philippe Peyrillé (philippe.peyrille@meteo.fr)

Key Points:

- Tropical waves are key to build the atmospheric environment conducive to an extreme precipitation event
- Equatorial Rossby waves appear as a new driver of extreme rainfall in the Central Sahel when combined with African Easterly Waves
- The combination of African Easterly Wave with an equatorial Rossby Wave and / or Kelvin wave, increase the probability of extreme rainfall

Abstract

Extreme precipitation events (EPE) are often associated with severe floods and significant damages in Central Sahel. To better understand their formation and improve their forecasts, we investigate the sub-seasonal drivers of EPEs. A composite analysis reveals that moist, cyclonic and upper-level divergence anomalies are found on average as a result of several tropical waves. The equatorial Rossby wave (ER) dominates at large scale providing a moist and convectively-active anomaly over the northern Sahel together with a smaller-scale African Easterly Wave (AEW). The Madden-Julian Oscillation provides upper-level divergence anomalies and a Kelvin wave increases convection during the EPE. Statistics show the prevalence of AEW and emphasize ER as a key driver of EPE. The co-occurrences of several tropical waves, especially those involving AEW, ER and Kelvin waves, increase the probability of EPE. Monitoring these tropical waves combinations could improve EPEs forecasts.

Plain Language Summary

The drivers of extreme precipitation events (EPE) over the Central Sahel are studied at subseasonal scales. A statistical approach is adopted to build an average extreme rainfall event. EPEs occur within a large-scale moist anomaly, an upper-level divergence, and at shorter scales an intense vortex. These features are provided by multiple tropical meteorological systems, called tropical waves, that have typical spatio-temporal scales greater than that of a convective storm. The four tropical waves studied here contribute to this favorable environment. However two of them – an Equatorial Rossby wave, rather slow, and an African Easterly Wave (more rapid) - explain the largest part of the favorable conditions leading to an EPE. Statistics show that a single intense AEW or the combination of multiple tropical waves increases the probability of EPE. Monitoring these tropical waves combinations could improve EPEs forecasts.

1 Introduction

Mesoscale convective systems provide most of the rainfall over the Central Sahel during the monsoon season (Mathon et al. 2002). The most intense of them produce very large amounts of precipitation in a short period of time (typically one day or less), leading to Extreme Precipitation Events (EPEs) that frequently result in severe socioeconomic damages (Di Baldassarre et al. 2010; Descroix et al. 2018). Though, EPEs remain a phenomenon difficult to anticipate as indicated by the poor capacity of current numerical weather prediction models in quantitatively forecasting rainfall (Vogel et al. 2018). A better understanding of their driving mechanisms, from days to weeks before the EPE, may help inform and develop relevant early warning systems by effectively indicating on potential large-scale precursors.

On subseasonal timescales (typically between 2 and 90 days), tropical waves might stand as possible precursors for EPE given their recognized role in modulating convection and rainfall in the tropics and West Africa (Kiladis et al. 2009, Schluter et al. 2019). However, little is known about their role in the occurrence of EPEs. The objective of the present study is to determine to what extent tropical waves drive the occurrence of EPEs.

The Madden-Julian Oscillation (MJO) is one of the subseasonal drivers of Sahelian rainfall that has received the greatest interest. EPEs are more likely during its low-level westerly phase (Sossa et al. 2017) or during its upper-level divergent phase (Schreck 2021). Aside from these studies, the understanding of Sahelian EPEs at subseasonal scale relies on the findings from very few case studies. They emphasize the importance of a humid environment with vertically-integrated water vapor contents (precipitable water hereafter) greater than 45-50 mm and of an intense synoptic disturbance such as an African Easterly Wave (AEW –Lafore et al. 2017, Maranan et al. 2019, Vizy and Cook 2022, Taylor et al. 2017). Other than the individual effect of tropical waves, the co-occurrence of several convectively-coupled waves has been observed during the record-breaking EPE that occurred on September 1st 2009 in Ouagadougou, Burkina Faso (Lafore et al. 2017). An active MJO and an equatorial Rossby wave (ER) were active at the time of the EPE together with a Kelvin wave and an intense AEW, well-marked in humidity and vorticity. There is however no study about the frequency of such a configuration in the occurrence of EPEs.

The present work investigates the subseasonal atmospheric conditions associated with Sahelian EPEs and assesses the contribution of tropical waves to their occurrence from a statistical point of view.

2 Data and methods

2.1 Definition and detection of EPEs

EPEs are defined here as events for which the 1°x1° daily rainfall exceeds the 99th all-day percentile. For their detection, we rely on a 142 rain-gauge rather dense network covering Burkina Faso over the 1995-2016 period without missing data (Sanogo et al. 2022). This dataset is preferred to any currently available gridded precipitation product given their difficulty in reproducing high rain rates (Satgé et al. 2020, Sanogo et al. 2022), thereby leading to numerous false detections. Following Sanogo et al. (2022), the daily rainfall measurements from rain gauges are aggregated at the scale of 1°x1° pixels, considering only pixels that have a minimum of five rain gauges (15 1°x1° pixels in total). The 99th all-day percentiles of these 15 time series range between 20 and 32 mm d^{-1} (see Text S1 and Figure S1 in Supporting Information – SI – for further details).

2.2 Datasets for characterizing the EPE large-scale environment

The atmospheric state associated with EPEs is documented based on the daily / 0.75° x 0.75° ERA Interim reanalysis data (Dee et al. 2011). Following previous studies on tropical waves (e.g., Schlueter et al. 2019, Wheeler et Kiladis 1999), the daily 2.5°x2.5° Outgoing Long-wave Radiation (OLR) from National Oceanic and Atmospheric Administration (NOAA, Liebmann and Smith 1996) is used to detect and characterize convectively-coupled waves and the convective activity at large scale.

The large-scale spatial distribution of the precipitation field is also qualitatively characterized with CHIRPS precipitation daily data (Funk et al. 2015) provided at a 1°x1° resolution by Roca et al. (2019). Similar results are found with other rainfall gridded products (not shown).

2.3 Tropical wave analysis

For a given parameter X, we compute the difference between its raw daily data and a smoothed daily climatology, in which only the first four harmonics are retained (Lafore et al. 2017, Roundy and Franck 2004). The resulting anomaly is detrended on a 90-day window centered on the EPE occurrence to only retain the intraseasonal part of the signal.

The contribution of four tropical waves – the MJO, ER, Kelvin wave and AEW – to the intraseasonal anomaly X* is quantified for several atmospheric fields using wave-number-frequency filtering, following Wheeler and Kiladis (1999) and Roundy and Franck (2004). The filtering process allows writing X* as $X^*=X^{MJO}+X^{ER}+X^{Kelvin}+X^{AEW}$ +residual, where the right-hand side terms are the wave-filtered contributions and a residual term of weak magnitude given the prevalence of the four waves considered here over West Africa). The filtering domains used for each tropical wave are standard (see Text S2 and Figure S2 in SI) and allows to isolate their signal without any overlap among then.

The filtering domain for theoretical shallow water waves are set up using equivalent depths between 12 and 90 m to identify the lower and upper bounds for the dispersion curves. The filtering domains used here are broadly similar to Schreck et al. (2012). The Kelvin wave domain is given by wave-number k and period T in [1,14]; [2.5-17.5 days]. The periods considered for Equatorial Rossby waves (ER) are [10-48 days] following Wheeler and Kiladis (1999). The MJO contribution is extracted from a domain encompassing periods from 30 to 96 days and wave-numbers 0 to 9. The (AEW) domain includes westward-propagating signals with wave-numbers -20 to -8 and periods between 2 and 10 days. Previous studies indicated a possible overlap between AEW and Mixed-Rossby Gravity waves (MRG) domains (Schlueter et al. 2019), such that the contribution of MRG are not considered here. . The other tropical waves considered here have well-separated filtering domains avoiding any overlap between MJO, ER, Kelvin wave and AEW.

The wavenumber–frequency filtering is applied to different parameters – OLR, precipitable water, velocity potential, vorticity and wind – to account for the different signatures of tropical waves in the atmosphere with a specific attention on OLR, as a measure of the convectively-coupled nature of the waves.

2.4 EPE attribution to tropical waves

Inspired by similar work on tropical cyclones (Landu et al. 2020, Chen and Chou 2014, Schreck et al. 2011, 2012, Feng et al. 2023), EPEs are attributed to a given convectively-active wave depending on the magnitude of its wave-filtered anomaly. Convectively-active waves are first detected when the wave-filtered OLR anomaly averaged over a 5° box centered at the EPE location is greater than half of the box-averaged standard deviation following previous studies by Landu et al. (2020), Chen and Chou (2014) and Feng et al. (2023). The leading contribution of tropical waves to EPEs and their modulations of the EPE probability remain similar for thresholds of -0.3 and -1 standard deviation (see Text S4 and Figure S3 in SI for details).

The contribution of each tropical wave and of multiple waves combinations are determined. As we consider four tropical waves, 16 combinations of active tropical waves are possible: four with one active wave only, six combing two waves, four combing three waves, one combining the four waves and a last category with no active wave (NONE). Each day or each EPE is attributed to a unique tropical wave combination.

We then quantify the modulation of the EPE occurrence by each wave combination by the change in EPE frequency of occurrence (Xavier et al. 2015, Guigma et al. 2021). It is given by the relationship $\Delta P^{EPE}_{wave}=(P^{EPE}_{wave} - P^{EPE}_{all\text{-}day}) / P^{EPE}_{all\text{-}day} *100$ where P^{EPE}_{wave} is the probability of EPE occurrence during a given tropical wave combination. It is given by the number of EPEs during which the given tropical wave combination occurs divided by the total number of days during which this combination is observed in the climatology, regardless of EPEs. $P^{EPE}_{all\text{-}day}$ is the probability of EPE occurrence computed for all days from the climatology and corresponds to 0.01 given EPE definition (days with precipitation exceeding the 99th all-day percentile). Results from the attribution of EPE to tropical waves are tested following a bootstrap procedure at the 95 % confidence level (details in Text S4 and Figure S3 in SI).

2.5 Composite

Once the dates of EPE occurrence are obtained, the atmospheric fields are aligned in time and space (latitude and longitude) relative to the time and location of each EPE, providing the basis for an EPE composite analysis (i.e. "average EPE”). DAY 0 refers to the day of occurrence of the composite EPE and its composite location is set to the average EPE location [2°W,12.5 °N]. Only values of the composite passing a two-tailed test at the 95 % confidence level are displayed in the results presented here (see Text S4 in SI for further details).

3 Results

3.1 Atmospheric conditions leading to EPEs

Figure 1 shows the composite state of the atmosphere during the days surrounding the composite EPE. The precipitation associated with EPE is initiated ~10° further to the east at DAY-1 (Fig. 1d). It then moves westward to reach the EPE location at DAY 0 with a value greater than 15 mm d^{-1} in CHIRPS data (Fig. 1d-g-j). It occurs within an upper-level large-scale divergence anomaly, developing several days before the EPE (Fig1. a-j), and a low-level cyclonic vortex that forms near DAY 0, which induces north-westerly wind anomalies to the west of Burkina Faso (Fig. 1g). The EPE is associated with a large-scale humid and convectively-active anomaly (> 3000 km) arriving from the north-eastern part of the Sahel (Fig.1 b-e-h-k). A synoptic vortex of smaller scale (< 1000 km) develops to the west of the moist anomaly at DAY-1 before increasing at DAY 0 and DAY+1. A noticeable convective anomaly is also found in the Atlantic Ocean at DAY-3 moving westward near the Guinea Coast at DAY-1 and around the EPE location at DAY 0. The cyclonic anomaly is also visible, on average, over the 925-600-hPa layer to the east of the mean EPE location (Fig. 1c-f-i), indicating a deep and barotropic vortex. It is associated with a high precipitable water value, up to 47 mm (~70% column relative humidity, not shown).

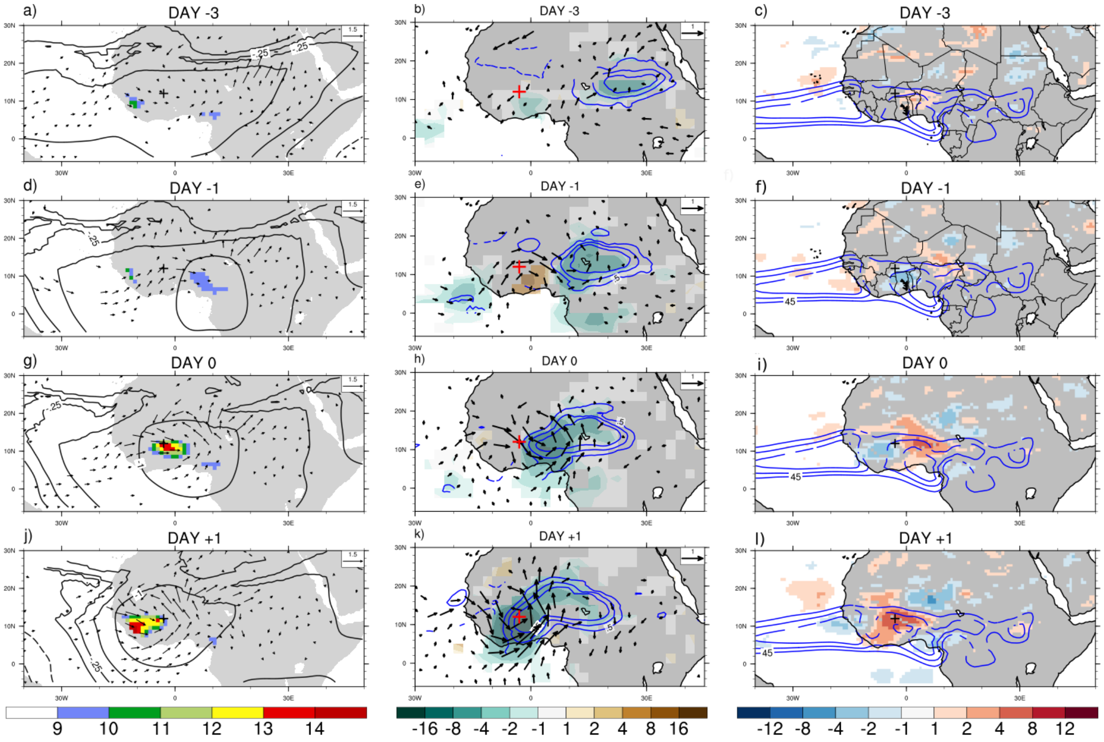

Figure 1 : Left column: EPE composite mean of the 925-hPa horizontal wind anomalies (vectors), 200-hPa negative (divergent) velocity potential anomalies (one contour every 0.2 x10^6 m^2s^{-1}) and CHIRPS raw precipitation (shading, m d^{-1}). Lags are expressed in days relative to the occurrence of the composite EPE. Latitude and longitude are relative to the EPE mean location indicated by the black cross. Middle column: same as left column except for OLR anomalies (shading, W m^{-2}), precipitable water anomalies (one contour every 0.5 kg m^{-2}) and 925-600 hPalayer-averaged wind (vectors, m s^{-1}). Right column: same as left column except for 925-600-hPa mean relative vorticity anomalies (shading, s^{-1}) and raw precipitable water (contour every 2.5 kg m^{-2} from 45 kg m^{-2}). Only statistically significant values at the 95 % confidence level are displayed.

The average conditions emphasized by the composite consists in the co-occurrence of a multi-scale pattern. They confirm and extend previous results from the literature based on case studies (Lafore et al. 2017, Maranan et al. 2019) by pointing out the significance of a synoptic scale vortex (~1000 km) and a larger-scale moist anomaly (> 3 000 km) during EPEs.

3.2 Contribution of tropical waves to the EPE large-scale environment

To further understand the origin of such an atmospheric environment, the intraseasonal anomalies of OLR, precipitable water and winds are split into contributions from individual tropical waves (Fig. 2). The large-scale moist and convective envelope results from an ER visible at DAY-1 near 15°E-15°N that slowly propagates westward. It is associated with a large-scale cyclonic circulation to the west of the moist anomaly resulting in westerlies at the EPE location, which increases the southwesterly monsoon flow. The synoptic cyclonic vortex is the signature of an AEW that develops at DAY-1 with a convectively-active phase at 10°E and a convectively-suppressed phase at the EPE location. Finally, a convectively-coupled Kelvin wave signal propagates eastward with a peak of convective activity slightly west of the EPE location at DAY 0. It provides westerly wind anomalies.

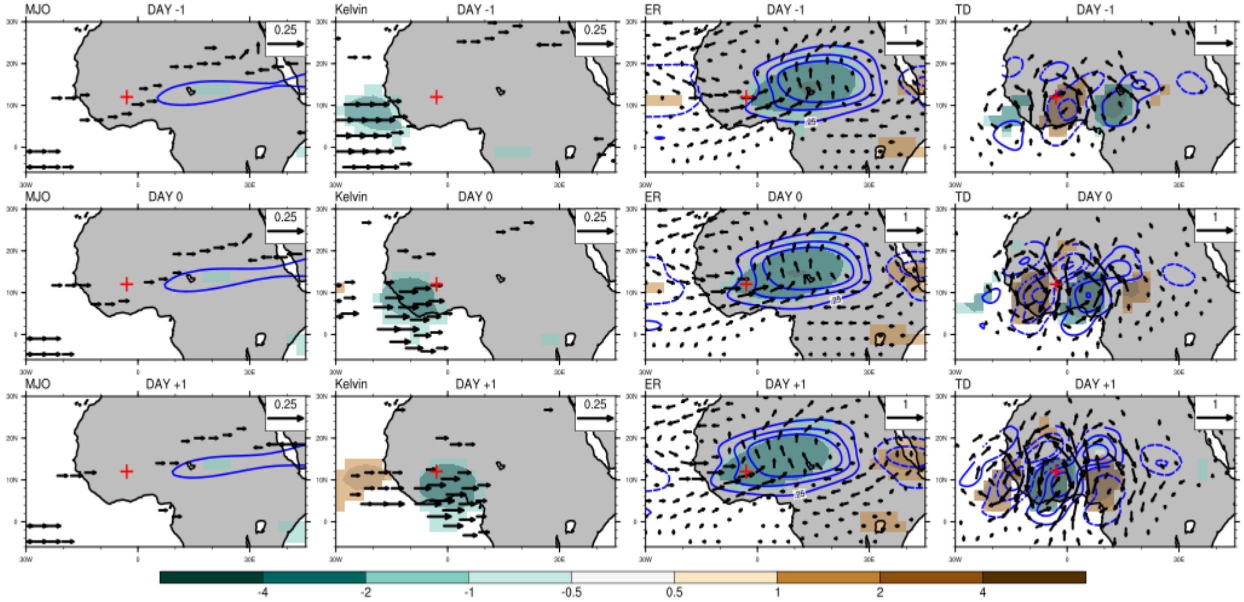

Figure 2 : Contributions of tropical waves to the EPE composite mean based on wavenumber-frequency-filtered OLR anomalies (shading, W m^{-2}), precipitable water anomalies (blue contours, one contour every 0.25 kg m^{-2}) and 925-600 hPa ~~layer~~averaged wind (vectors, m s^{-1}), for the Madden-Julian Oscillation (MJO, first column), Kelvin wave (KW, second column), Equatorial Rossby wave (ER, third column) and African Easterly Waves (AEW, last column). Lags are expressed in days relative to the composite EPE. The red cross indicates the average location of the composite EPE. Only statistically significant values at the 95 % confidence level are displayed.

The phasing of different waves is further documented using hovmoller diagrams centered around the EPE location (Fig. 3). The ER and AEW are the major contributors to the large-scale envelope of negative OLR anomalies (shading, Fig. 4a). The ER (red contour) is key to strengthen deep convection 5 to 10 days prior to the EPE. It is clearly seen in the unfiltered intraseasonal anomaly (shading). The Kelvin wave (blue) is also an important contributor at a shorter scale. It is visible three days in advance over the Atlantic Ocean and enhances convection to the west of the EPE at DAY 0. The signature of the MJO is weak for OLR and is better detected on velocity potential (Fig. 3b). A large-scale upper-level divergence anomaly prevails over the Sahel with a dominant contribution from the MJO and to a lesser extent the ER and the Kelvin wave (Fig. 3b). The evolution of precipitable water and vorticity intraseasonal anomalies are similar (Fig. 3c,d) and indicate that the moist cyclonic anomaly coming from the east is associated with an ER signal at large scale (red contours) and an intense AEW at shorter scale (green contours).

To summarize, the anomalous mean conditions associated with EPEs result from the co-occurrence of several tropical waves with a group of westward propagating convectively-coupled waves, well-marked in vorticity and humidity (ER and AEW) crossing a second group of eastward propagating waves (MJO and Kelvin wave) well-marked in upper-level divergence.

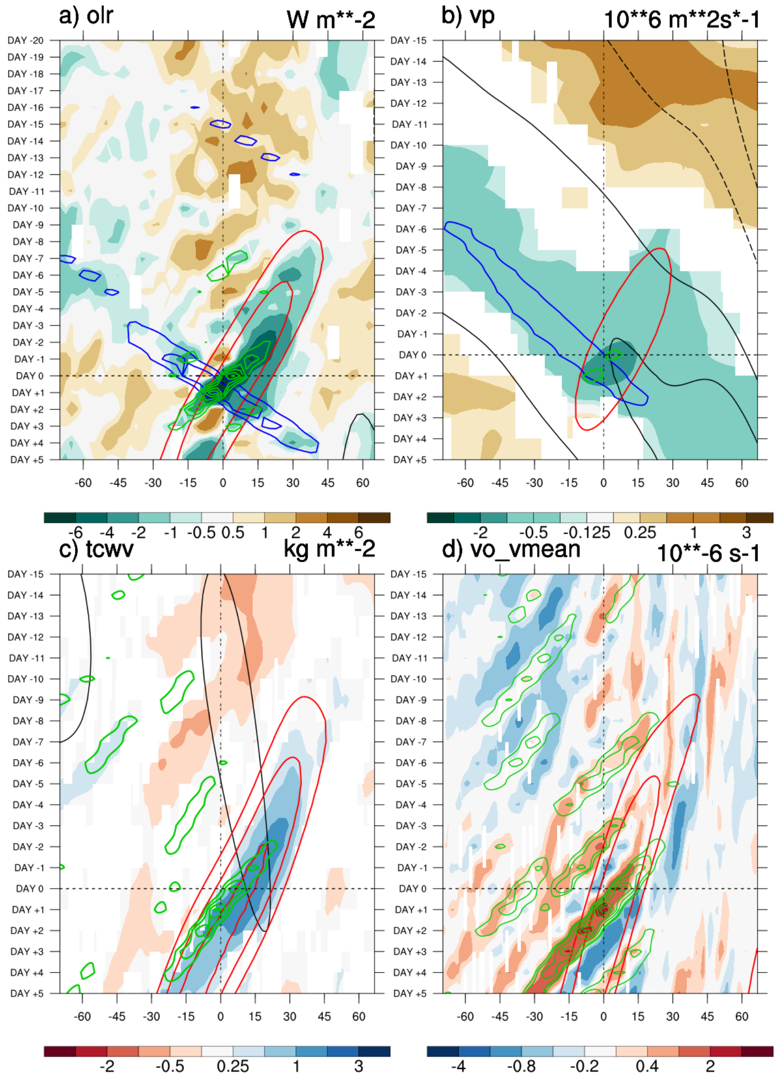

Figure 3 : (a) Lag - longitude hovmoller diagram of the composite anomalies of OLR (W m^{-2} shading) averaged between -2.5° to +2.5° N relative to the EPE location. The contours indicate the wavenumber-frequency-filtered OLR anomalies of the tropical waves (contours every 1 W m^{-2}): the MJO (black), Equatorial Rossby wave (red), Kelvin waves (blue) and AEWs (green). Only the convectively-active component of the waves is shown (negative OLR anomalies only). DAY 0 corresponds to the day of occurrence of EPE and longitudes are relative to the mean EPE location. (b), (c) and (d) same as (a) except for 200-hPa velocity potential (m^2 s^{-1}, one contour every -1.25 x10^5 m^2 s^{-1}), precipitable water (kg m^{-2}, contour every 0.2 kg m^{-2}) and 925-650 hPa

mean relative vorticity (s^{-1}, contour every 0.25 x10^{-6} s^{-1}), respectively. Only statistically significant values at the 95 % confidence level are displayed.

3.3 Co-occurrence of tropical waves during EPEs

Figure 4a shows the total contribution of each tropical wave to the occurrence of EPEs. The AEWs are the leading drivers for EPE with broadly half the EPEs associated with an AEW. The contributions of ER and Kelvin waves are also statistically significant and are active in more than 35% of EPE. It confirms their leading role as drivers of EPEs. The contributions of the MJO although not statistically significant, represents more than 20 of EPEs, suggesting that the four waves are frequent enough to co-occur.

Figure 4b refines this view by displaying the percentage of EPEs attributed to each possible combination of waves. The x-axis indicates the 16 possible combinations of active tropical waves. The first four bars (red) indicate that a single active AEW has the greatest contribution among the single-wave category (16%). The total contribution of the single wave category accounts for 39.3 % of EPEs leaving 44.7% of them attributed to the combination of multiple tropical waves. Only 16% of EPEs are not associated with any wave. Statistically significant contributions are found for the combinations ER+AEW and AEW+Kelvin wave (yellow bars), ER+Kelvin+AEW (blue) and MJO+Kelvin+AEW. Finally, 1.5% of EPEs occur within a combination of the four tropical waves (green).

Figure 4c further assesses the modulation of the EPE frequency of occurrence by each wave combination compared to the wave climatological occurrence. Four combinations of active tropical waves clearly emerge, all including the combination of an AEW, an ER and / or a Kelvin wave. The wave combination ER+Kelvin+AEW shows the most significant increase indicating that combining westerly and easterly tropical waves clearly favors the EPE occurrence. In contrast the occurrence of a single intense AEW is the only one-wave configuration that increases EPE probability. The combinations of waves identified here as key modulators of EPE occurrence are not sensitive to an increase or decrease in the threshold for a convectively-active wave detection indicating that our results are robust Only the contribution of the AEW-alone configuration increases with the threshold while the contributions of the four-wave combination is slightly reduced (see text S4 and Figure S3 in SI).

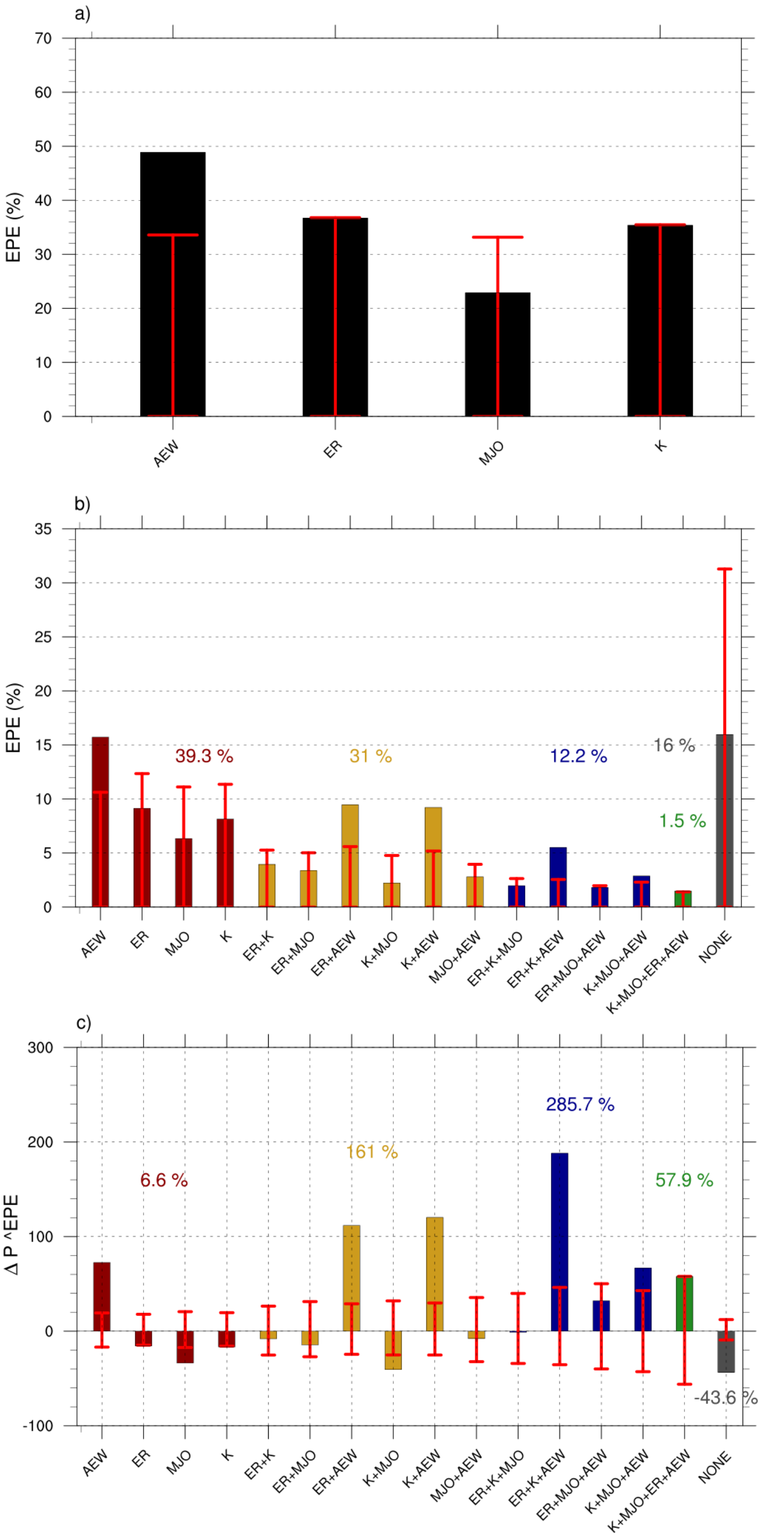
a)
EPE (%)
0
10
20
30
40
50
60
70
AEW
ER
MJO
K
b)
EPE (%)
0
5
10
15
20
25
30
35
39.3 %
31 %
12.2 %
16 %
1.5 %
AEW
ER
MJO
K
ER+K
ER+MJO
ER+AEW
K+MJO
K+AEW
MJO+AEW
ER+K+MJO
ER+K+AEW
ER+MJO+AEW
K+MJO+AEW
K+MJO+ER+AEW
NONE
c)
Δ P ^EPE
-100
0
100
200
300
6.6 %
161 %
285.7 %
57.9 %
-43.6 %
AEW
ER
MJO
K
ER+K
ER+MJO
ER+AEW
K+MJO
K+AEW
MJO+AEW
ER+K+MJO
ER+K+AEW
ER+MJO+AEW
K+MJO+AEW
K+MJO+ER+AEW
NONE

Figure 4: Percentage of EPE attributed to (a) each tropical wave and (b) to each configuration of tropical waves (single waves and combinations of waves). (c) Percentage change in EPE frequency of occurrence for a given wave configuration (ΔP^{EPE}). In (b) and (c), colored bars indicate configurations with a single active wave (red), with exactly two active waves (yellow), with exactly three active waves (blue), with four active waves (green) and no active wave (none, gray). The colored percentages indicate the total contribution or percentage of change of each wave configuration. The red vertical lines indicate the 95 % significance level.

4 Conclusions

This study demonstrates that the atmospheric environment of EPEs occurring over Burkina Faso, and most probably over Central Sahel, consists, on average, in a large-scale moist envelope propagating westward and an upper-level divergence anomaly, in which an intense cyclonic vortex generates northerlies at the EPE location. It confirms and extends previous results based on case studies (Lafore et al. 2017, Engel et al. 2017). The role of tropical waves was then investigated. To our knowledge, it is the first study that provides statistical evidence on the role of tropical waves in EPE occurrence, in particular the role of tropical wave co-occurrence.

The contribution of tropical waves can be summarized as follows:

- The equatorial Rossby wave is the dominant driver at large scale of the convective, moist anomalies developing over the eastern Sahel 5 days prior to the EPEs. Previous studies investigated the role of ER wave only on precipitation subseasonal variability over West Africa (Mounier et al. 2008, Janicot et al. 2010, Roehrig et al. 2011) but to our knowledge, the leading role of ER waves in Sahelian EPE occurrence is a new finding.
- AEW have a major contribution to EPE. A strong AEW, which frequently develops within an ER envelope, generates a deep moist cyclonic vortex.
- The MJO provides upper-level divergence and favors convection over the Central and Eastern Sahel during the week before EPE occurrence, in agreement with previous studies (Schreck 2021, Sossa et al. 2017).
- A Kelvin wave increases convection, the low-level westerlies and upper-level divergence at the time of EPE.

Statistics conditional to the occurrence of EPEs show that the AEW and ER are the most frequent tropical waves associated with EPEs. The wave configurations increasing the EPE frequency of occurrence are the single AEW and the combinations of an AEW with an ER and / or a Kelvin wave. This emphasizes the importance of tropical wave co-occurrence for EPEs. The physical processes involved in such configurations and the way they contribute to the occurrence of an EPE should be addressed in the future.

This study has strong implications for anticipating EPE at subseasonal scale, since large-scale tropical waves have significant predictability at lead time beyond a few days. A better predictability of EPE over the Central Sahel might thus be gained by monitoring their propagation and their potentiality to occur in combination with an AEW. It can provide guidance for analyzing forecasts and help weather forecasters to issue early warnings of high-impact weather systems in the Central Sahel. This in turn would allow better preparedness for and response to EPEs, reducing risk of injuries, damages and economical loss.

Acknowledgments

We thank K. Schreck and the anonymous reviewer for the constructive feedback on the manuscript during the review process.

Data Availability Statement

All data used in this manuscript are publicly available. NOAA Interpolated Outgoing Longwave Radiation (OLR) data provided by the NOAA PSL, Boulder, Colorado, USA, from their website at https://psl.noaa.gov/data/gridded/data.olrcdr.interp.html . The EPE dates for the 15 1°x1° pixels used in this study for compositing are available at https://doi.org/10.5281/zenodo.7764390.

ERA Interim reanalysis data is accessible at ECMWF website https://www.ecmwf.int/en/forecasts/dataset/ecmwf-reanalysis-interim. CHIRPS data can be obtained at https://doi.org/10.14768/06337394-73A9-407C-9997-0E380DAC5598.

References

Chen, G., and C. Chou, 2014: Joint Contribution of Multiple Equatorial Waves to Tropical Cyclogenesis over the Western North Pacific. *Mon. Wea. Rev.*, **142**, 79–93, https://doi.org/10.1175/MWR-D-13-00207.1.

Dee, D.P., Uppala, S.M., Simmons, A.J., Berrisford, P., Poli, P., Kobayashi, S., Andrae, U., Balmaseda, M.A., Balsamo, G., Bauer, P., Bechtold, P., Beljaars, A.C.M., van de Berg, L., Bidlot, J., Bormann, N., Delsol, C., Dragani, R., Fuentes, M., Geer, A.J., Haimberger, L., Healy, S.B., Hersbach, H., Hólm, E.V., Isaksen, L., Kållberg, P., Köhler, M., Matricardi, M., McNally, A.P., Monge-Sanz, B.M., Morcrette, J.-.-J., Park, B.-.-K., Peubey, C., de Rosnay, P., Tavolato, C., Thépaut, J.-.-N. and Vitart, F. (2011), The ERA-Interim reanalysis: configuration and performance of the data assimilation system. Q.J.R. Meteorol. Soc., 137: 553-597. https://doi.org/10.1002/qj.828

Descroix, L., and Coauthors, 2018: Evolution of surface hydrology in the Sahelo-Sudanian Strip: An updated review. Water, 10, 748, https://doi.org/10.3390/w10060748.

Di Baldassarre, G. D., A. Montanari, H. Lins, D. Koutsoyiannis, L. Brandimarte, and G. Blöschl, 2010: Flood fatalities in Africa: From diagnosis to mitigation. Geophys. Res. Lett., 37, L22402, https://doi.org/10.1029/2010GL045467.

Engel, T., A. Fink, P. Knippertz Extreme Flooding in the West African Cities of Dakar and Ouagadougou – Atmospheric Dynamics and Implications for Flood Risk Assessments, vol. 19 (2017), p. 11983

Funk, C., Peterson, P., Landsfeld, M. *et al.* The climate hazards infrared precipitation with stations—a new environmental record for monitoring extremes. *Sci Data* **2**, 150066 (2015). https://doi.org/10.1038/sdata.2015.66

Feng, X., Yang, GY., Hodges, K.I. *et al.* Equatorial waves as useful precursors to tropical cyclone occurrence and intensification. *Nat Commun* **14**, 511 (2023). https://doi.org/10.1038/s41467-023-36055-5

Guigma, K.H., Guichard, F., Todd, M. *et al.* Atmospheric tropical modes are important drivers of Sahelian springtime heatwaves. *Clim Dyn* **56**, 1967–1987 (2021). https://doi-org.insu.bib.cnrs.fr/10.1007/s00382-020-05569-9

Janicot, S., F. Mounier, S. Gervois, B. Sultan, and G. N. Kiladis, 2010: The Dynamics of the West African Monsoon. Part V: The Detection and Role of the Dominant Modes of Convectively Coupled Equatorial Rossby Waves. J. Climate, 23, 4005-4024, https://doi.org/10.1175/2010JCLI3221.1.

Kiladis G, Wheeler M, Haertel P, Straub K, Roundy P. 2009. Convectively coupled equatorial waves. Rev. Geophys. 47: RG2003, DOI:10.1029/2008RG000266.

Lafore, J.-P., Beucher F., Peyrillé P., N. Chapelon, D. Bouniol, G. Caniaux, F. Favot A multi-scale analysis of the extreme rain event of Ouagadougou in 2009, Q. J. R. Meteorol. Soc., 143 (2017), pp. 3094-3109

Landu, K., Goyal, R. & Keshav, B.S. Role of multiple equatorial waves on cyclogenesis over Bay of Bengal. *Clim Dyn* **54**, 2287–2296 (2020). https://doi.org/10.1007/s00382-019-05112-5

Liebmann B, and C.A. Smith 1996. Description of a complete (interpolated) outgoing longwave radiation dataset. Bull. Am. Meteorol. Soc. 77: 1275–1277

Maranan, M., Fink, A. H., Knippertz, P., Francis, S. D., Akpo, A. B., Jegede, G., & Yorke, C. (2019). Interactions between Convection and a Moist Vortex Associated with an Extreme Rainfall Event over Southern West Africa, *Monthly Weather Review*, *147*(7), 2309-2328. Retrieved Oct 6, 2022, from https://journals.ametsoc.org/view/journals/mwre/147/7/mwr-d-18-0396.1.xml

Mathon, V., H. Laurent, and T. Lebel, 2002: Mesoscale convective system rainfall in the Sahel. J. Appl. Meteor. Climatol., 41, 1081–1092, https://doi.org/10.1175/1520-0450(2002)041,1081: MCSRIT.2.0.CO;2.

Mounier, F., S. Janicot, and G. N. Kiladis, 2008: The West African monsoon dynamics. Part III: The quasi-biweekly zonal dipole. J. Climate, 21, 1911-1928, https://doi.org/10.1175/2007JCLI1706.1.

Roehrig, R., F. Chauvin, and J. Lafore, 2011: 10–25-Day Intraseasonal Variability of Convection over the Sahel: A Role of the Saharan Heat Low and Midlatitudes. *J. Climate*, **24**, 5863–5878, https://doi.org/10.1175/2011JCLI3960.1.

Roundy P. E. andW.M. Frank, 2004. A climatology of waves in the equatorial region. J. Atmos. Sci. 61: 2105–2132.

Roca, R., Alexander, L. V., Potter, G., Bador, M., Jucá, R., Contractor, S., Bosilovich, M. G., and Cloché, S.: FROGS: a daily 1° × 1° gridded precipitation database of rain gauge, satellite and reanalysis products, Earth Syst. Sci. Data, 11, 1017-1035, https://doi.org/10.5194/essd-11-1017-2019, **2019**.

Sanogo, S., Peyrillé, P., Roehrig, R., Guichard, F., & Ouedraogo, O. (2022). Extreme Precipitating Events in Satellite and Rain Gauge Products over the Sahel, *Journal of Climate*, *35*(6), 1915-1938. Retrieved Oct 6, 2022, from https://journals.ametsoc.org/view/journals/clim/35/6/JCLI-D-21-0390.1.xml

Satgé, F., D. Defrance, B. Sultan, M.-P. Bonnet, F. Seyler, N. Rouché, F. Pierron, and J.-E. Paturel, 2020: Evaluation of 23 gridded precipitation datasets across West Africa. J. Hydrol., 581, 124412, https://doi.org/10.1016/j.jhydrol.2019.124412.

Schlueter, A., Fink, A. H., Knippertz, P., & Vogel, P. (2019). A Systematic Comparison of Tropical Waves over Northern Africa. Part I: Influence on Rainfall, *Journal of Climate*, *32*(5), 1501-1523. Retrieved Oct 6, 2022, from https://journals.ametsoc.org/view/journals/clim/32/5/jcli-d-18-0173.1.xml

Schreck, C. J., J. Molinari, and K. I. Mohr, 2011: Attributing tropical cyclogenesis to equatorial waves in the western North Pacific. J. Atmos. Sci., 68, 195-209, https://doi.org/10.1175/2010JAS3396.1.

Schreck, C. J., J. Molinari, and A. Aiyyer, 2012: A global view of equatorial waves and tropical cyclogenesis. Mon. Wea. Rev., 140, 774-788, https://doi.org/10.1175/MWR-D-11-00110.1.

Schreck, C. J., III. (2021). Global survey of the MJO and extreme precipitation. Geophysical Research Letters, 48, e2021GL094691. https://doi.org/10.1029/2021GL094691

Sossa, A., Liebmann, B., Bladé, I., Allured, D., Hendon, H. H., Peterson, P., & Hoell, A. (2017). Statistical Connection between the Madden–Julian Oscillation and Large Daily Precipitation Events in West Africa, *Journal of Climate*, *30*(6), 1999-2010. Retrieved Oct 6, 2022, from https://journals.ametsoc.org/view/journals/clim/30/6/jcli-d-16-0144.1.xml

Taylor, C., Belušić, D., Guichard, F. *et al.* Frequency of extreme Sahelian storms tripled since 1982 in satellite observations. *Nature* **544**, 475–478 (2017). https://doi.org/10.1038/nature22069

Vizy, E.K., Cook, K.H. Distribution of extreme rainfall events and their environmental controls in the West African Sahel and Soudan. *Clim Dyn* 59, 997–1026 (2022). https://doi.org/10.1007/s00382-022-06171-x

Vogel, P., Knippertz, P., Fink, A. H., Schlueter, A., and Gneiting, T. (2018). Skill of Global Raw and Postprocessed Ensemble Predictions of Rainfall over Northern Tropical Africa. *Weather and Forecasting* 33, 2, 369-388, available from:https://doi.org/10.1175/WAF-D-17-0127.1

Wheeler, M. and G. N. Kiladis, 1999. Convectively coupled equatorial waves: Analysis of clouds and temperature in the wavenumber–frequency domain. J. Atmos. Sci. 56: 374–399, **https://doi.org/10.1175/1520-0469(1999)056<0374:CCEWAO>2.0.CO;2.**

Xavier, P., Rahmat, R., Cheong, W. K., and Wallace, E. (2014), Influence of Madden-Julian Oscillation on Southeast Asia rainfall extremes: Observations and predictability, *Geophys. Res. Lett.*, 41, 4406–4412, doi:10.1002/2014GL060241.

References From the Supporting Information

Gosset, M., M. Alcoba, R. Roca, S. Cloché, and G. Urbani, 2018: Evaluation of TAPEER daily estimates and other GPM-era products against dense gauge networks in West Africa, analysing ground reference uncertainty. Quart. J. Roy. Meteor. Soc., 144 (Suppl. 1), 255–269, https://doi.org/10.1002/qj.3335

Schreck, C. J., III. (2015). Kelvin Waves and Tropical Cyclogenesis: A Global Survey, *Monthly Weather Review*, *143*(10), 3996-4011. Retrieved Feb 28, 2023, from https://journals.ametsoc.org/view/journals/mwre/143/10/mwr-d-15-0111.1.xml

Straub, K. H., and G. N. Kiladis, 2002: Observations of a convectively coupled Kelvin wave in the eastern Pacific ITCZ. *J. Atmos. Sci.*, **59**, 30–53.

[Geophysical Research Letters]

Supporting Information for

Tropical Waves are key drivers of Extreme Precipitation Events in the Central Sahel

Philippe Peyrillé[1], Romain Roehrig[1], and Sidiki Sanogo[1,2]

[1]Centre National de Recherches Météorologiques, Météo-France, CNRS, Université de Toulouse, 42 Avenue Coriolis, 31057 Toulouse, France

[2]Institut Pierre-Simon Laplace, Sorbonne université / CNRS, 4 place Jussieu, 75005 Paris, France

Contents of this file

Texts S1 to S4
Figures S1 to S3

Introduction

The supplementary information presents details on the rain-gauge dataset used to detect Extreme Precipitating Events (EPE – Text S1 and Fig. S1), on the identification of tropical waves (Text S2 and Fig. S2), the inference of statistical significance for EPE composites and EPE attribution to tropical wave configurations (Text S3), and the sensitivity of EPE wave attribution to the threshold used to detect tropical waves (Text S4 and Fig. S3).

Text S1: Rain-gauge based precipitation dataset over Burkina Faso.

The dataset used to detect extreme precipitation event is built from 142 rain-gauge stations covering most of Burkina Faso (Fig. S1, see also Sanogo et al. 2022). They provide daily accumulated precipitation summaries over the period 1995–2016. Considering a 1°x1° resolution grid covering Burkina Faso (Fig. S1), the rain-gauge network often exhibits more than five stations within each 1° x 1° pixel. The densest pixel encompasses 15 stations. Following Gosset et al. (2018), we only considered 1°x1° pixels that contain at least five stations, and thus ensure a proper estimate of precipitation characteristics at this scale. The daily 1°x1° rain-gauge-based precipitation dataset over Burkina Faso is derived as the arithmetic mean of the rainfall records from all the stations encompassed within each 1°x1° pixel. Based on this gridded dataset, the 99th all-day percentile is used as a rainfall threshold to detect EPEs. Figure S1 shows that it ranges between 20 to 32 mm d^{-1}, broadly equivalent to rainfall events of 50 mm at the station scale (not shown).

Text S2: Tropical waves identifications.

The domains for filtering tropical waves are illustrated with Figure S2, which shows the normalized wavenumber-frequency spectrum for OLR in the 15°S- 15°N band.

It is obtained as in Wheeler and Kiladis (1999) by dividing the OLR spectrum by a red noise estimate of the background spectrum, regardless of equatorial symmetry (Roundy and Frank 2004, Straub and Kiladis 2002). Spectral peaks of energy appear where enhanced variability of OLR emerges from the background noise. Filtering domains for tropical waves are derived from this spectrum to enclose the spectral peaks of energy associated with the different waves and are indicated by the solid polygons in Figures S2. Although slight variations of the filtering domains can be found among various authors, results presented here are insensitive to reasonable variations in the filtering domains.

Text S3: Statistical significance of EPE composites and attribution to tropical wave configurations.

The statistical significance of the EPE composite mean is assessed against the null hypothesis that the composite anomalies are obtained because of random variability. We use a bootstrap approach similar to Schreck (2015). The null hypothesis is tested by generating a series of 500 random samples of the same size as our EPE ensemble. Each sample is built as follows:

1. An EPE is randomly selected from the EPE dataset with replacement. We select the day and month from this EPE but randomly select a year from a different EPE without replacement.

2. We then randomly select another EPE case from the EPE dataset with replacement and use its latitude / longitude to build the composite.
3. These steps are repeated to generate a sample of the same size as the initial EPE composite dataset.

A given parameter is then averaged among this ”null” sample to obtain a composite mean. The whole procedure is repeated 500 times to produce an ensemble of 500 null composite means obtained from random variability. At each data point, the statistical significance of the EPE composite mean is evaluated against the null composite mean by using a two-tailed test at the 95% confidence level. The EPE composite mean is considered statistically significant when it is either greater than the 97.5th percentile or lesser than the 2.5th percentile of the null composite mean. Only values passing this test are displayed and analyzed.

The statistical significance of the percentage of EPE attributed to tropical waves and of the corresponding change in EPE probability are tested against the null hypothesis that they could have arisen from random variability. The percentage of days from the climatology during which a given wave or wave combination is active is first computed for all pixels using the criterion of attribution based on box-averaged wave-filtered OLR (not shown). For a given wave or wave combination that is active during N days of the all-pixel climatology, 500 random samples of the same size N are generated from the climatology. The corresponding precipitation and the 99th percentile are used to determine the number of EPEs associated to each of the 500 samples, which form a null distribution that is associated with random variability. The random change in EPE probability is also deduced for each sample.

The percentage of EPEs attributed to a given combination is considered statistically significant at the 95% level when it is greater than the 95th percentile of this random distribution. The change in EPE probability for a given wave combination is considered statistically significant at the 95 % confidence level when its either larger than the 97.5th percentile or smaller than the 2.5th percentile of the corresponding null distribution.

Text S4: Sensitivity of EPE attribution to the threshold used for tropical wave detection.

The threshold to detect any convectively-active tropical wave is discussed here. A threshold of -0.5 box-averaged standard deviation of wave-filtered OLR anomaly is used to identify whether a given tropical wave is convectively-active or not. The sensitivity of our results to this threshold is presented in Figure S3 which is the same as Figure 4 presented in the article except for thresholds of -0.3 and -1 standard deviations. In the main manuscript, we aligned with the somewhat arbitrary threshold of -0.5 which is often used in the literature seeking to attribute tropical cyclones to tropical waves (Chen and Chou 2014, Landu et al. 2020, Feng et al. 2023). Raw thresholds on OLR wave-filtered anomalies have also been tested for wave detection, leading to the similar conclusions (not shown).

Figures S3a,b show that AEW, ER and Kelvin waves remain the leading tropical waves contributing to EPE occurrence with decreasing contribution when the detection threshold is increased. The statistical significance of the Kelvin waves is slightly below the 95% confidence level compared to results presented in Figure 4. It is expected that the increase (decrease) of the detection threshold should yield a reduction (increase) of attributed EPEs as the number of detected waves diminishes. When a threshold of -0.3 standard deviation is used, the wave combinations that have the greatest contribution to EPEs and the largest modulation of EPE probability are similar to those obtained with a threshold of -0.5 standard deviation: single AEW, ER+AEW, K+AEW, ER+K+AEW and MJO+K+ER+AEW (Fig. S3b,c). The contribution of the combination of four waves is increased with a more significant change in EPE probability while the combination of K+MJO+AEW falls under the threshold of statistical significance. For a threshold of -1 standard deviation, multiple wave combinations become less likely (Fig. S3e). Although the key combinations for EPE occurrence remain qualitatively similar, the single (intense) AEW configuration now dominates as well as the contribution of single ERs (Fig. S3e). The percentage change in EPE probability remains however close to the one presented in the manuscript with the same key wave combinations with the largest modulations. The main change is a strongest effect of single AEW and a weaker effect of the four-wave combination.

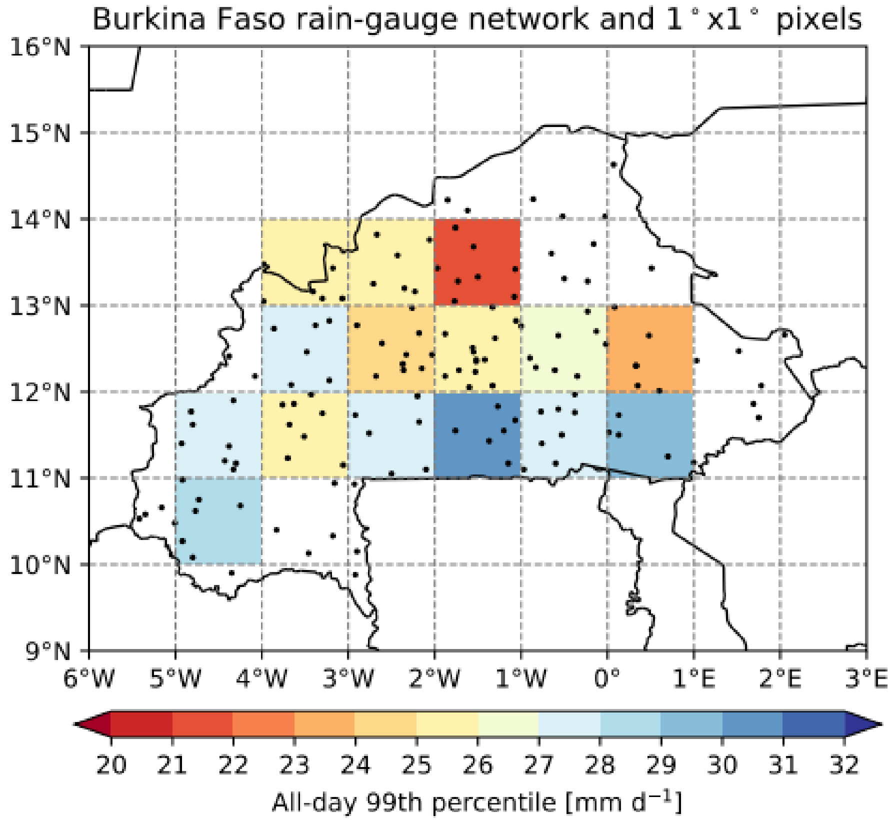

Figure S1: Spatial distribution of the rain gauges used in the study (dots) and 99th all-day percentile of precipitation (mm d^{-1}, shading). The 99th percentile is computed for 1°x1° pixels over the [1996-2015] period (adapted from Sanogo et al. 2022).

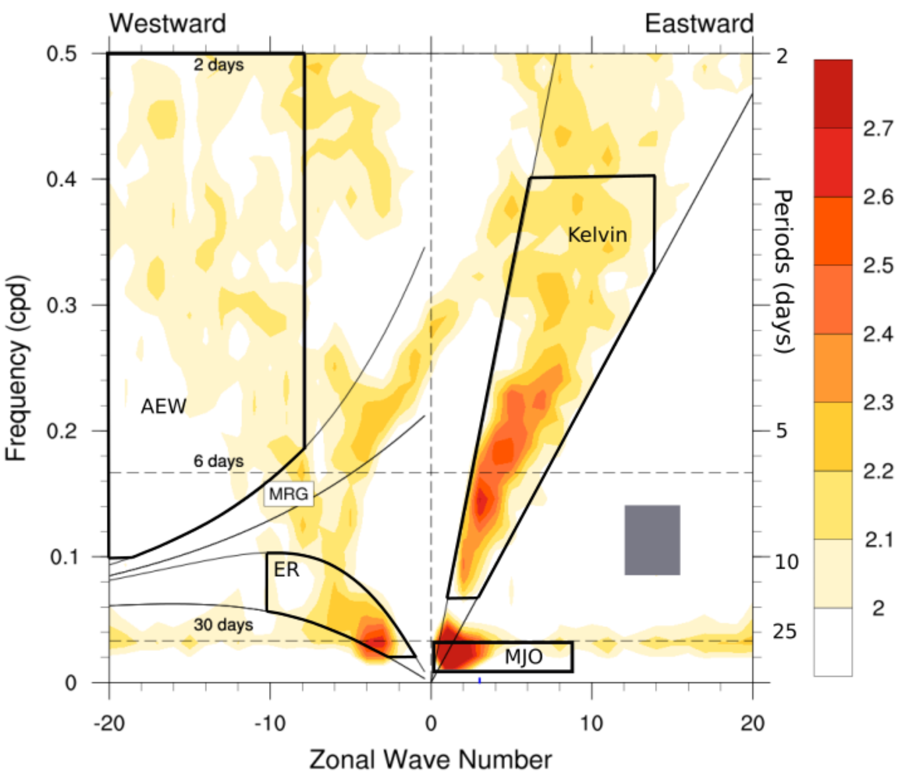

Figure S2: Normalized wavenumber-frequency spectrum of NOAA Interpolated daily OLR from 1996 to 2016, between 15° S and 15°N, and without equatorial symmetry consideration. The bold solid polygons indicate domains for the filtering of MJO, Kelvin wave, ER and AEW. The thin solid lines indicate the dispersion curve for the equivalent depths of 12 and 90 m. The gray rectangle hides an artificial peak generated by aliasing from the satellite swath path size and frequency (see Wheeler and Kiladis 1999 and Roundy and Franck 2004).

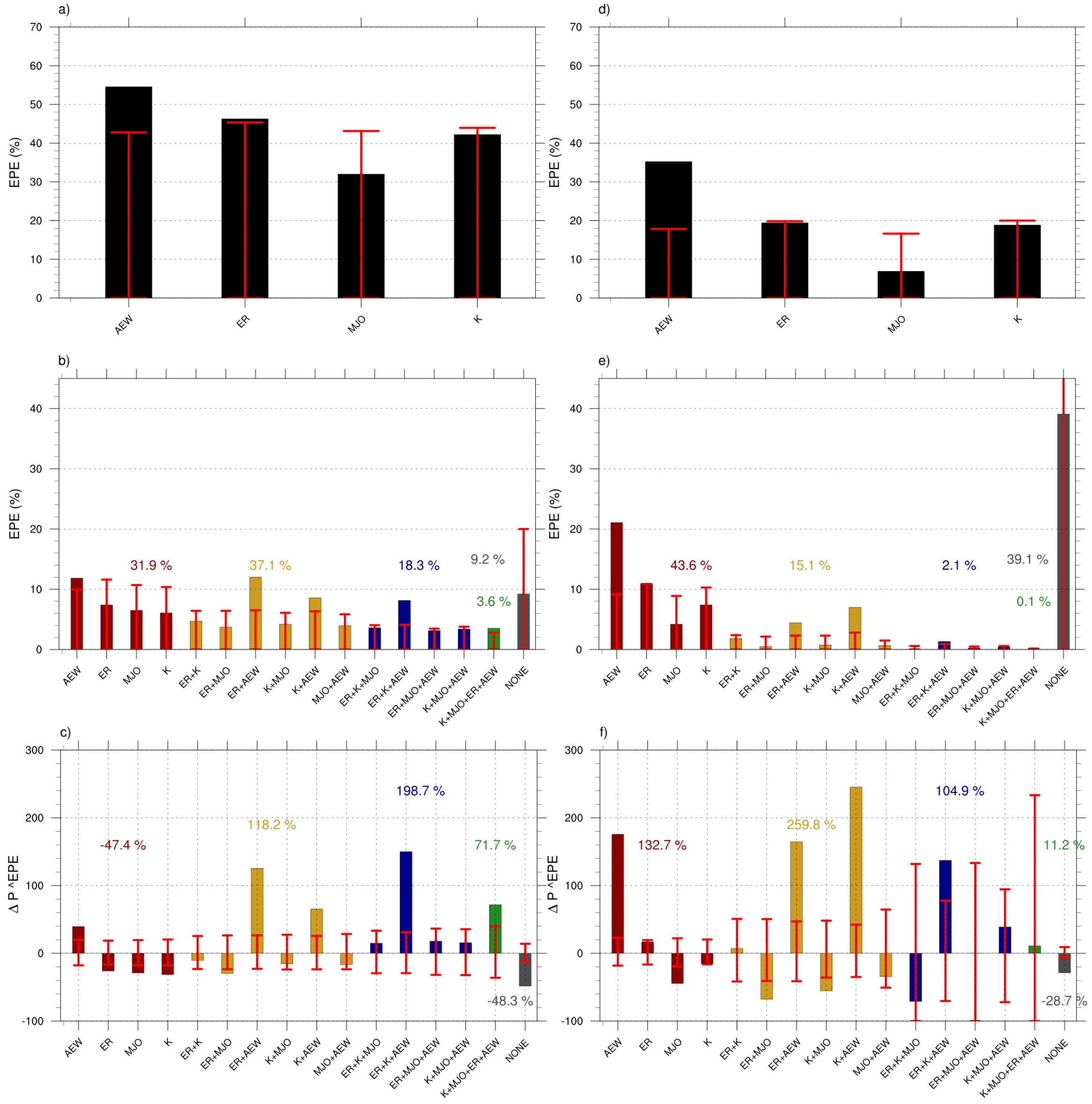

Figure S3: Percentages of EPEs attributed to (a) each tropical wave, (b) to each combination of tropical waves and (c) percentage change in EPE frequency of occurrence for a given wave combination obtained using a threshold of -0.3 standard deviation to detect active tropical waves. (d, e, f) same as (a, b, c) except a threshold of -1 standard deviation threshold is used to detect active tropical waves. The red vertical lines indicate the interval below the 95 % significance level.